IEEE IAS annual meeting, Hong Kong, CDROM proc., 2-6 oct. 2005

Electromagnetic resonant generator

M. Ruellan, S. Turri, Hamid Ben Ahmed and B. Multon
SATIE UMR CNRS 8029
Brittany Branch ENS de Cachan
ruellan@bretagne.ens-cachan.fr

Abstract **- In this paper, the authors present the energy production potential of a mechanically-resonant electrical generator system, which makes use of natural human walking movements.**

The characteristics associated with the human walk will be discussed first, followed by the electromechanical modeling approach employed. The choice of electromechanical architecture will be justified and the permanent magnet and moving coil structure can then be modeled and optimized. A demonstration device has also been generated and tested in order to validate the concept developed as well as the theoretical models derived.

Index Terms **- Human-powered systems, low-power electronics, electromechanical generator, permanent magnet machine, optimization.**

I. INTRODUCTION

In order to reduce the need for batteries or for recharging accumulators on the electric grid, it appears increasingly worthwhile to seek available energy resources from within the human environment. From this perspective, several research teams have over the past few years been working on the design of generators able to recover energy from human movements [1,2,3].

The movements that may be used for producing energy consist of two types:

- those performed naturally. The "Kinetics" watches manufactured by Seiko (see Fig. 1), which recover a portion of the energy from human movement thanks to an original generator configuration, would provide an example of this type;

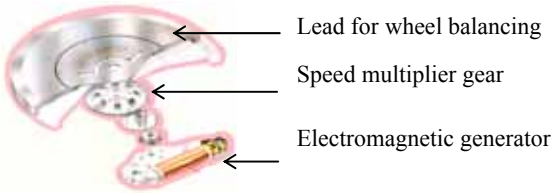

Fig. 1: Diagram of the electrical generator used in Seiko's Kinetics watch

- those performed for a specific purpose, which carries with it the disadvantage of imposing upon the individual to be mobile during the action phase and which may cause human fatigue. We can cite, within this category, the systems (portable lamps, radios, etc.) manufactured by the Freeplay company. Such objects operate with a crank-type system.

In this article, the authors will present the energy-production potential of a linear, mechanically-resonant electrical generator system, which makes use of natural walking movements in order to yield a power of approximately 100 mW, capable for example of being used to recharge a cell phone.

This system operates on the basis of a principle that resembles the Kinetics watch system, which must produce infinitely greater power and (as we are hoping) direct actuation. It thus became essential to design a new and more powerful device, via a system operating with an accumulator and behaving like a charger. The accumulator component will not be studied herein; it is modeled as an ultimately variable voltage source.

The characteristics associated with the human walk will be discussed first, followed by a presentation of an electromechanical modeling approach for the purpose of determining the energy potential of such a system. The choice of electromagnetic generator architecture is then carried out and the permanent magnet and moving coil structure will be modeled. The electromechanical system, which includes a spring and whose mobile mass is composed of the generator winding, gets optimized next. Lastly, we will display the demonstration device developed along with a number of experimental results.

The originality of this study lies both in the strong coupling between mechanical and electromagnetic aspects and in the optimization of the non-controlled system.

II. THE WALKING MOTION

We have considered the movements of the hip during walking motion, since electronic devices are often carried either around the waist or in a purse/bag.

This movement is three-dimensional and may be decomposed along the three component axes: lateral (x), longitudinal (y) and vertical (z).

Figure 2 shows the 2D hip movement along the y and z component axes.

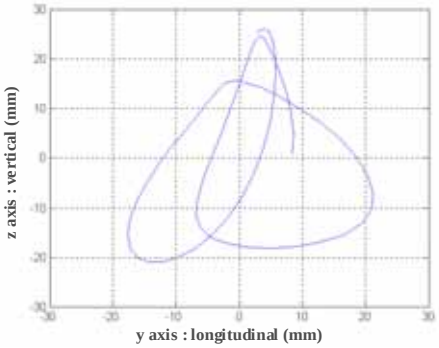

Fig. 2: 2D walking movements at 5 km/hr (2-step representation)

Depending on the desired components, several types of generators may be designed: rotation with the y and z

components, translation with just the *z* component, etc.

We are proposing herein to make use of the most regular component and the one that most closely traces the sine curve : the vertical component. Moreover, it would appear that its frequency varies only by a little with respect to walking speed, as one's speed gets adjusted to the actual walking step length.

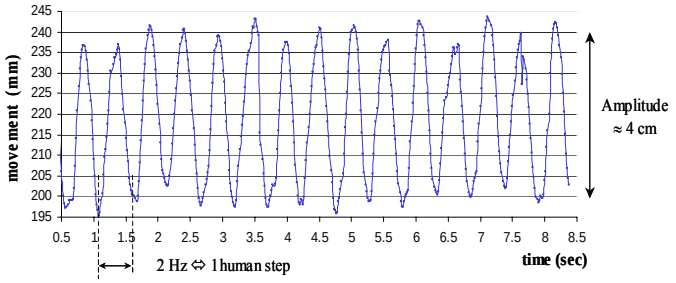

Fig. 3: Vertical right hip movements (z component) while walking at 5 km/hr

Given the information depicted in Figure 3, we will now consider, within the scope of a preliminary design, the vertical hip movement as a quasi-sinusoidal source with an imposed peak-to-peak amplitude and frequency:

$$h(t) = Z_M . \cos(\omega_{step} . t) \qquad (1)$$

with Z_M equal to approximately 2.10^{-2} m and an f_{step} on the order of 2 Hz.

This hypothesis is verified as long as the portable generator does not cause any discomfort to the pedestrian. It is thus essential that its total mass and hence the energy discharged remain sufficiently low. The acceptable level has not been evaluated herein.

III. POTENTIAL ENERGY RECOVERY FROM THE RESONANT GENERATOR

A. *Principle and general structure*

The system, in its theoretical version, is composed of a small box attached to the human body by means of a belt fastened around the waist, in which a flyweight (consisting of the mobile part of the linear electromechanical generator) moves suspended between two springs. Figure 4 shows a schematic diagram that allows formulating a set of mechanical equations. This system will function at a frequency near its eigenfrequency or resonance frequency when activated by the walker's hip movement. The mobile mass will be composed of the mobile part of the electromagnetic generator and damped by the production of electrical energy.

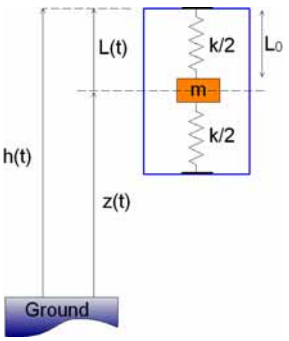

Fig. 4: Mechanical diagram

This simplified representation gives rise to a simple mechanical approach and remains valid regardless of the final mechanical solution selected (plate springs, helical springs, rotational springs, etc.). The movement of mass *m* is governed by the following equation (2):

$$m.\frac{d^2L_1(t)}{dt^2} = m.\frac{d^2h(t)}{dt^2} - F_i - k.L_1(t) \qquad (2)$$

with:

$$L_1(t) = L(t) - L_0 - \frac{m.g}{k} \qquad (3)$$

k is the equivalent stiffness of the entire spring system.

The mechanical losses by internal friction are neglected at this level of study yet may be easily reintroduced subsequently.

In order to streamline the notations, in the following discussion we will use L(t) instead of $L_1(t)$.

F_i is the reaction force exerted by the electromagnetic generator when its energy is being discharged.

In this initial general electromechanical study, we will consider a force variation law $F_i(t)$ of the viscous friction type (see Figure 5 below):

$$F_i = \lambda \cdot \left(\frac{dL}{dt}\right) \qquad (4)$$

where λ is an "active damping coefficient" that depends on both the generator geometry and the value of the charge.

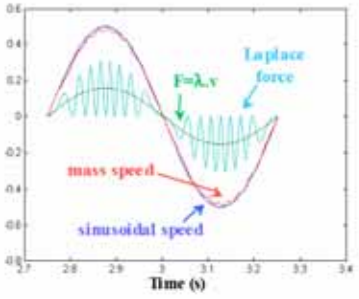

Fig. 5: Actual and equivalent Laplace forces and speeds

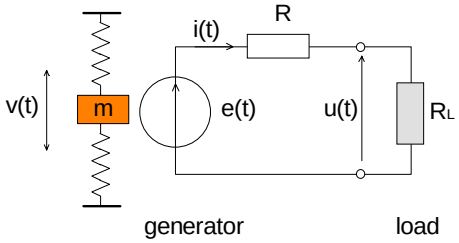

Fig. 6: Schematic diagram of the energy conversion process

B. *Operations at mechanical resonance*

Mechanical resonance is obtained at the excitation angular frequency, such that: $\omega_{step} = \omega_0 = \sqrt{\frac{k}{m}}$.

Under these conditions, the extracted power equals [4]:

$$P_0 = \frac{m.Z_M.\omega_{step}^{\ 3}.L_{max}}{2} \qquad (5)$$

where L_{max} is the stroke, i.e. the amplitude of displacement of the mobile mass (between the equilibrium position of the mobile mass and both the upper and lower stops imposed by the box).

With the optimal active damping coefficient:

$$\lambda_{opt} = \frac{mZ_M \omega_{step}}{L_{max}} \qquad (6)$$

C. Operations with varying excitation frequency

Let's now display results for an example in which the mechanical resonance frequency is not tuned to the walking step frequency f_{step}.

By means of simulation, we have been able to obtain the results presented in Figure 7; for a given resonance frequency f_0 of the mass-spring system, the power recovered is always increasing with walking step frequency f_{step}. This increases however will always be less than that obtained had the system been synchronized at frequency f_{step} (green curve).

In the example provided herein, the mobile mass *m* equals 50 grams, the stroke L_{max} 0.04 m and the excitation amplitude Z_M 0.02 m.

The electrical power obtained at resonance frequency varies as the cube of the excitation frequency, as set forth in Equation (5) above.

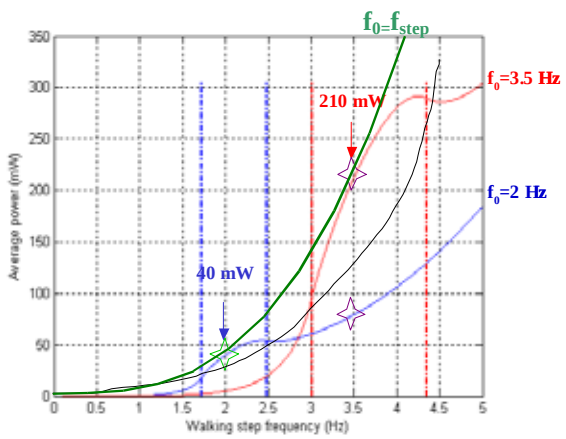

Fig. 7: Average power for $f_{generator} = f_0 = 2$ Hz and $f_0 = 3.5$ Hz at several walking step frequencies

IV. ELECTROMAGNETIC GENERATOR DESIGN

The electromagnetic generator has a synchronous permanent magnet and moving coil, tubular structure (Fig.8). Magnets have either axial (M^z) or radial (M^r) magnetization. This structure exhibits the advantage of being simple to produce, while minimizing the mobile mass and considerably reducing magnetic losses. Indeed, the main magnetic induction is due to permanent (fixed) magnets, making the variation of this induction in the magnetic circuit insignificant.

In order to achieve the necessary system optimization of the generator, we require analytical models that remain simple enough without sacrificing precision. For this reason, the following discussion will provide a description of the analytical modeling set-up used for our electromagnetic generator.

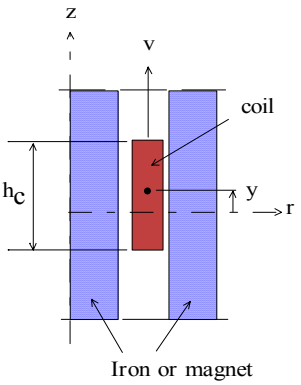

Fig. 8 axisymetric configuration

A. Analytical Modeling

From simplified generic analytical model adaptated to permanent magnet synchronous linear actuators [5], we studied three magnetic topologies of linear generator stator (Fig. 9).

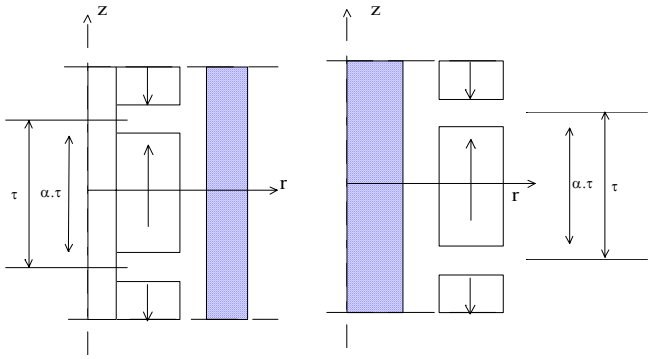

(a), (b) Axially magnetized machine topology

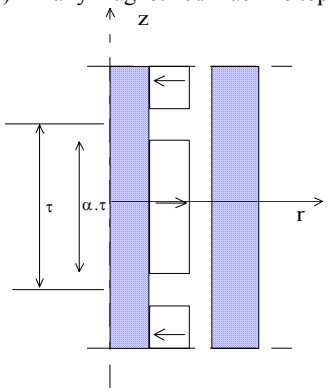

(c) Radially magnetized machine topology

Fig. 9: Elementary Configurations of the generator stator

This modeling approach has been applied on the basis of the following simplifying hypotheses:

- the materials used are presumed to be isotropic, with the physical characteristics such as permeability being constant within each sub-domain;
- the relationship between induction (flux density) and the magnetic field is linear (constant permeability);
- the magnetization M of the magnets is presumed constant and their demagnetization has not been

considered;
- the end effects are neglected, the axial length is presumed to be infinite with respect to the polar pitch.

The aim of this model is to compute electromagnetic force when coil generate a current in a resistive load. This force is hence proportionnal to spatial distribution of flux density and to the coil linear speed v.
Thanks to axisymmetrical geometry, distribution can be computed by potential vector $A(r,z)$:

$$\vec{A}(z,r) = \sum_{\bar{n}}^{\infty} \Psi_n(r).e^{jknz}.\vec{u}_\theta \quad (j^2=-1) \qquad (7)$$

where k is a propagation coefficient :

$$k = \frac{\pi}{\tau} \qquad (\tau \text{ is the polar pitch})$$

Full knowledge of potential vector at every point of computation domain means computation of radial distribution for each n^{th} rank harmonic « n » : $\Psi_n(r)$.

Thus we need to solve the Maxwell-Ampère vectorial equation :

$$\overrightarrow{rot}\left(\vec{H}\right) = 0 \qquad \text{(no current source)} \qquad (8)$$

The relations between the two quantities in this equation are :

$$\vec{B} = \mu.\vec{H} + \vec{M}$$

$$\vec{B} = \overrightarrow{rot}\left(\vec{A}\right) \qquad (\text{with } div(A) = 0)$$

Which gives the following relation :

$$-\frac{\partial^2\vec{A}}{\partial z^2} - \frac{\partial\vec{A}}{\partial r}\left(\frac{\vec{A}}{r} + \frac{\partial\vec{A}}{\partial r}\right) = \overrightarrow{rot}\left(\vec{M}\right) \qquad (9)$$

The magnetization distribution along the Z-axis can be expanded in Fourier's series :

$$M(z) = \sum_{n\ impair}^{\infty} \hat{M}_n.e^{jknz} \qquad (10a)$$

$$\text{with : } \hat{M}_n = \frac{4B_{rem}}{n.\pi}\sin\left(n\frac{\pi}{2}\alpha\right) \qquad (10b)$$

In the general situation, this magnetization can be divided into two parts :

$$\vec{M}(z) = \begin{cases} M^r(z) & \vec{u}r \\ M^z(z) & \vec{u}z \end{cases} \qquad (11)$$

Equation (9) becomes now :

$$\frac{\partial\Psi_n}{\partial u^2} + \frac{1}{u}.\frac{\partial\Psi_n}{\partial u} - \Psi_n\left(1+\frac{1}{u^2}\right) = \frac{j}{nk}\hat{M}_n^r \qquad (12)$$

with $u = nk.r$.

Thus, the solution of this differential equation can be written :

$$\Psi_n(u) = [\alpha_n(u) + c_n].I_1(u) + [\beta_n(u) + d_n].K_1(u) \qquad (13)$$

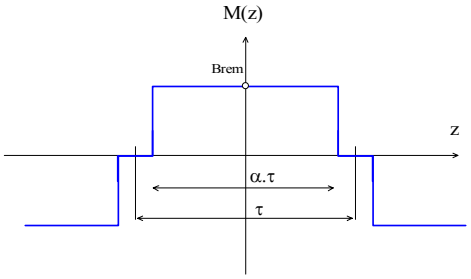

Fig. 10 Magnetization distribution

I_0 , I_1 are the modified bessel functions of the first kind, K_0 and K_1 are the modified bessel functions of the second kind, of order 0 and 1 respectively.

α_n et β_n are defined as follows :

$$\begin{cases} \alpha_{n(u)} = \frac{j\hat{M}_n^r}{nk}\left[\int \frac{K_1(u)}{I_0(u).K_1(u) - K_0(u).I_1(u)}du\right] \\ \beta_{n(u)} = \frac{j\hat{M}_n^r}{nk}\left[\int \frac{-I_1(u)}{I_0(u).K_1(u) - K_0(u).I_1(u)}du\right] \end{cases} \qquad (14)$$

c_n and d_n are constants determined from the interface conditions between subdomain (p) and adjacent subdomain (p + 1) :

$$\begin{cases} H_{z_{(p)}}\left(r = r_{(p)}\right) = H_{z_{(p+1)}}\left(r = r_{(p)}\right) \\ B_{r_{(p)}}\left(r = r_{(p)}\right) = B_{r_{(p+1)}}\left(r = r_{(p)}\right) \end{cases} \qquad (15a)$$

On top of that, two boundary conditions are added :

$$\begin{cases} A_\theta(r = 0) = 0 \\ A_\theta(r = \infty) = 0 \end{cases} \qquad (15b)$$

From equation (13) we can easily determine the three flux density components :

$$\vec{B} = \begin{vmatrix} -\frac{\partial A}{\partial z} & \vec{u}_r \\ 0 & \vec{u}_\theta \\ \frac{A}{r} + \frac{\partial A}{\partial r} & \vec{u}_z \end{vmatrix}$$

Which leads to :

$$B_{rn}(z,r) = -jkn\begin{Bmatrix} [\alpha_n(u) + c_n].I_1(u) \\ +[\beta_n(u) + d_n].K_1(u) \end{Bmatrix}.e^{jknz} \qquad (16a)$$

$$B_{zn}(z,r) = (n.k)\begin{Bmatrix} [\alpha_n(u) + c_n].I_0(u) \\ -[\beta_n(u) + d_n].K_0(u) \end{Bmatrix}.e^{jknz} \qquad (16b)$$

The small system dimensions and frequencies along with the large total magnetic air gap make the inductive effects in the coil negligible. Therefore, from an electrical point of view, the generator can be modeled by both an electromotive force e and a series internal resistance R . The load R_L is assumed to be purely resistive.

Under these conditions, the electromagnetic force $F_i(y)$ expression is directly derived from magnets' flux $\varphi_f(y)$ calculation :

$$F_i(y) = \frac{e.i}{v} = \left(\frac{d\varphi_f}{dy}\right)^2 \frac{v}{r\left(1+r_L^*\right)} \qquad (17)$$

where $r_L^* = R_L/R$ and $r = R/(n_s)^2$ (n_s is the coil's number of turns).

Magnets' flux per turn can be written as :

$$\varphi_n(y) = \frac{1}{h.(R_2-R_1)} \int_{y-h/2}^{y+h/2} \int_{R_1}^{R_2} A(z,r)\,dr\,dz$$

Which can be rewritten as :

$$\varphi_f(y) = \sum_{n\ impair}^{\infty} \varphi_{nMax}.\cos(nky) \qquad (18)$$

Taking into account moving coil winding direction (Fig. 10), the value of φ_{nMax} is given by :

$$\varphi_{nMax} = \frac{2\pi}{h_c.(R_2-R_1)}\left(\frac{1}{nk}\right)^2 .\Delta_n . \int_{nkR_1}^{nkR_2} \left[c_n.I_1(u) + d_n.K_1(u)\right].du$$

$$\Delta_n = \frac{4}{m\pi k}\sin\left(m\frac{\pi}{2}\right).\sum_m^{\infty}\left[\frac{\sin\left[k(m+n)h_c/2\right]}{(m+n)} + \frac{\sin\left[k(m-n)h_c/2\right]}{(m-n)}\right]$$

where R_1 and R_2 are the inner and outer radius of the moving coil respectively.

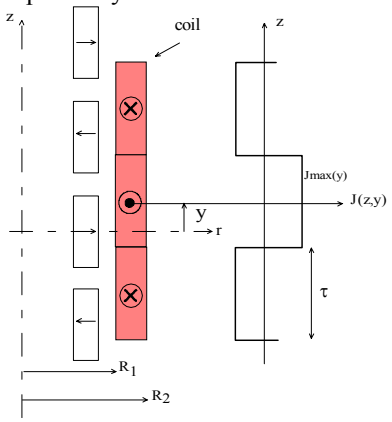

Fig. 11 Coil current density spatial distribution

The moving coil displacement and therefore the recovered power, are obtained from the force developed by the load-generator system by solving the mechanically-electrically-coupled differential equation (2). In this equation, mobile mass m is the coil mass.

B. Optimization

1) Principle

We present here the optimization of the generator dimensions and the spring stiffness (cf. Appendices A and B) considering the constraints of the mechanical excitation with the characteristics (ω_{step}, Z_m) with the double objective of maximizing the recovered power P_0 while minimizing the total mass M of the active parts (the box and spring masses have been neglected).

The task then consists of solving the following :

$$\min\left(M\left(x_j\right)\right) \text{ and } \max\left(P_0\left(x_j\right)\right)$$

with respect to :

$$g_i(x_j) \le 0 \begin{cases} g_1(x) = B_{a1}\text{-}B_{MAX} & B_{MAX}=1.2T \\ g_2(x) = B_{a2}\text{-}B_{MAX} & \\ g_3(x) = J\text{-}J_{MAX} & J_{MAX}=10^6 A.m^{-2} \\ g_4(x) = \tau - H & \\ g_5(x) = h_B - H & \text{cf. Appendix A} \end{cases}$$

Where x_j represent the optimization variables i.e the coil height (h_B), the magnet and coil weights (W_M and W_B), the pole pitch τ, α the ratio of a magnet to the pole pitch, r_L*, the interior and exterior yoke weights Y_1 and Y_2 and lastly the total height of the generator H.

The spring stiffness is set so that the eigenfrequency of the system will be equal to the excitation frequency (Fig 7):

$$k = \left(2.\pi.f_{step}\right)^2.m$$

This optimization is achieved with the NSGA-II genetic algorithm [6]. The principle of this algorithm is based on the ranking of the population individuals and the application of an elitist strategy. This ranking is carried out within the objective space and relies on the dominance as defined by Pareto. A diversity preserving mechanism is then applied in order to obtain an evenly crowded pareto front.

The figure 12 presents the general structure of this algorithm.

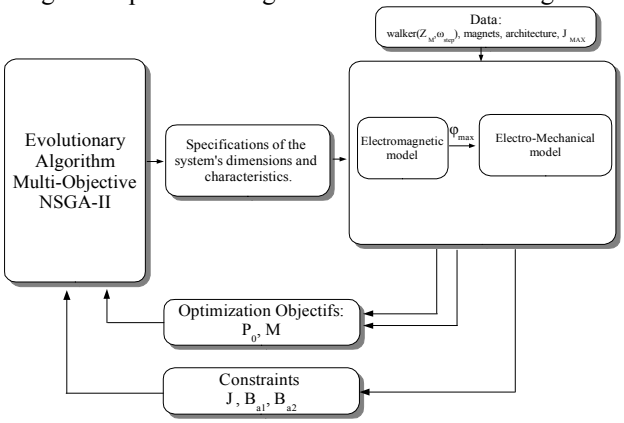

Fig. 12: General synoptic of optimization

2) Optimization results

We now turn to the results obtained with the different configurations shown in figure 9. The two optimized

objectives are described as a Pareto front (only the points which minimize the total active mass at fixed power are kept in the algorithm).

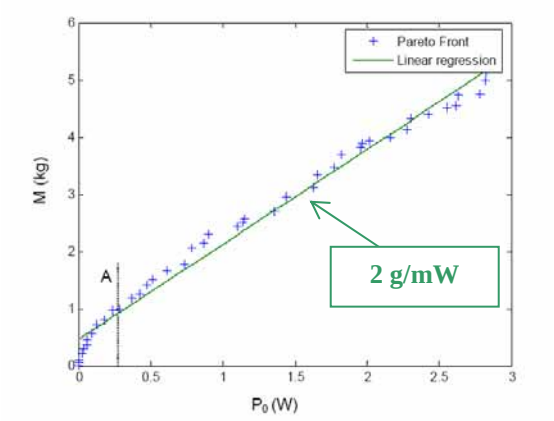

Fig. 13: Pareto Front for the (a) configuration .

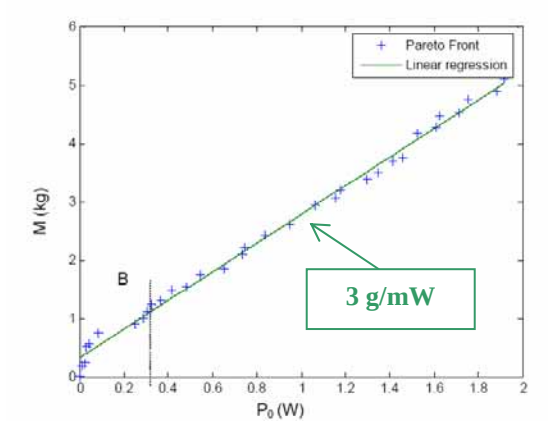

Fig. 14: Pareto Front for the (b) configuration.

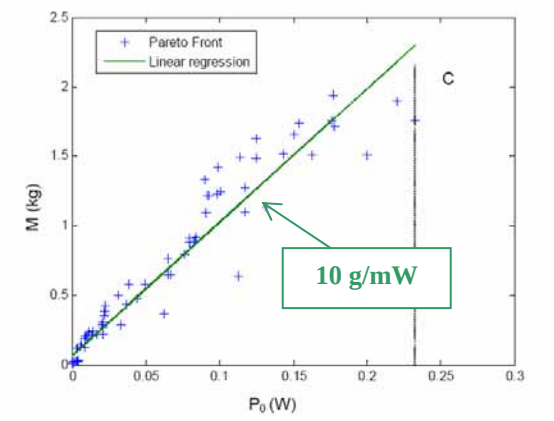

Fig. 15: Pareto Front for the (c) configuration

3) Results analysis

The optimization has revealed that the recovered power P_0 for an operation at the resonance is proportional to the total mass of the system as it is the case for the moving mass (Eq. 5).

Conversely, optimal normalized load resistance r_L^* is slightly dependent on recovered power. Its value is comprised between 2 and 10. These values result from a compromise between a high generator efficiency and a minimal mass.

Eventually, a performance comparison of the 3 generator topologies with optimal mass shows that for a given power P_0, the total mass is higher for configuration (c) as well as the overall dimension because its height is 30 mm larger than the ones obtained for configurations (a) and (b). Line slopes (obtained by linear regression) are also useful for comparison of these configurations.

Table 1 summarizes these results by giving the obtained dimensions for the three studied configurations and a recovered power of 250 mW. Figure 16 also provides a comparative schematic representation.

	Configuration (a)	Configuration (b)	Configuration (c)
W_M (mm)	2.7	2.0	2.8
W_C (mm)	13	35	8
α	0.8	0.8	0.7
h_C (mm)	19	5	9.7
τ (mm)	44	46	17.6
Y_1 (mm)	9.8	3	9.5
Y_2 (mm)	2	31	2.3
r_L*	2	4	4.3
H (mm)	164	163	199
P_0 (mW)	240	250	230
m (kg)	0.27	0.21	0,08
k (N/m)	42.5	33	12
M (kg)	0,96	0,9	1,75

Table 1 : Generator dimensions for a recovered power of around 250 mW

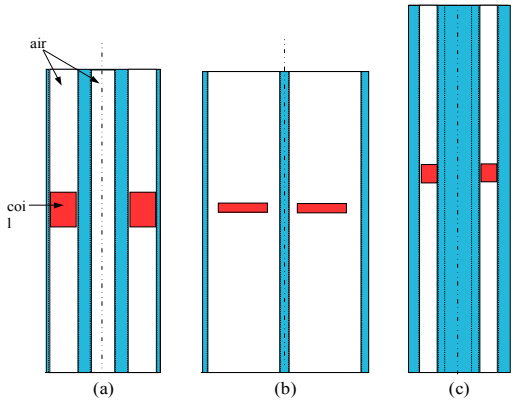

Fig. 16 : Optimal geometries comparison of the 3 configurations for Po=250 mW.

Total mass minimization, at fixed walking frequency (2 Hz) requires a very low spring stiffness (table 1) which leads to manufacturing difficulties : such springs are subject to buckling problems.

V. DEMONSTRATION DEVICE AND EXPERIMENTAL RESULTS

A. Electromagnetic structure choice for prototype

We chose an axially magnetized permanent magnet configuration, same as Fig. 9b, but with soft magnetic material pieces. Low cost ferrite (M = 0,39 T) permanent magnet was used and soft magnetic slices allow a flux concentration to improve air gap flux density and performances.

Sizes and material properties are summarized in appendix C.

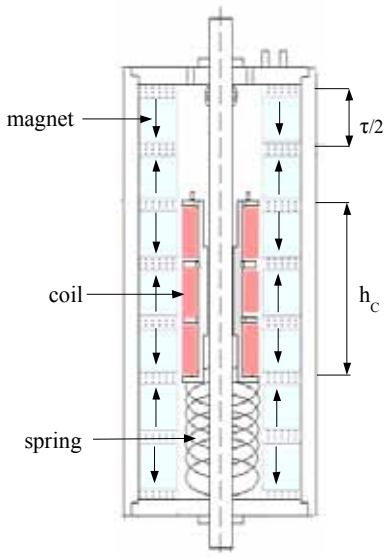

Fig. 17 : Scheme of electromagnetic mechanically resonant generator

Single phase coil (Fig. 18) is composed of three alternate windings in series (see Fig. 11). The height of each winding is equal to the polar pitch τ (total height of coil is : $h_c = 3.\ \tau$).

The electric wire diameter is 0,2 mm, coil resistance is equal to 45 Ω and its mass is equal to 50 grams.

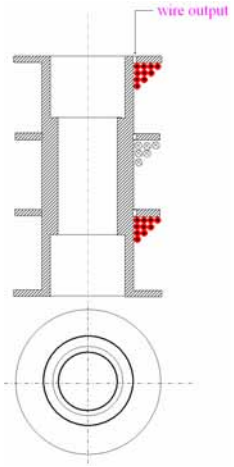

Fig. 18 :Scheme of moving coil

B. Experimental results

It prove impossible to make a spring with the desired stiffness (8 N/m) to adjust resonant frequency to walking movement (about 2 Hz). Such a spring led to important buckling problems. Since the objective was to validate the operating principle of the generator, we preferred to increase the eigenfrequency of the system by including a spring of better quality (a stiffness of 106 N/m). For the stiffer spring the resonant frequency becomes 7,3 Hz with a mobile mass of 50 g.

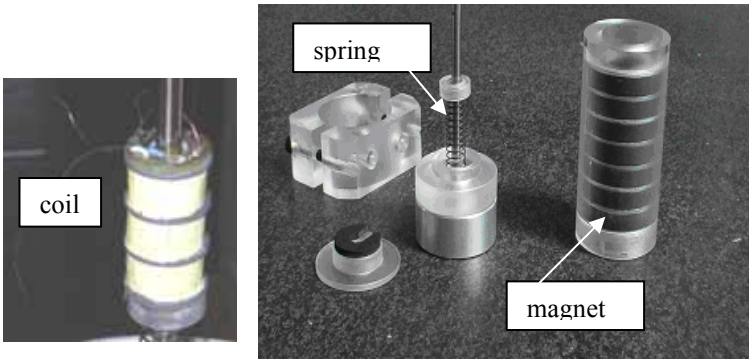

Fig.19 : Pictures of demonstrator parts.

A walking simulator (Fig. 20) has been designed and manfactured in order to conduct tests on the generator; this simulator is composed of two mobile axes, making it possible to reproduce the walking movement as shown in Figure 3.

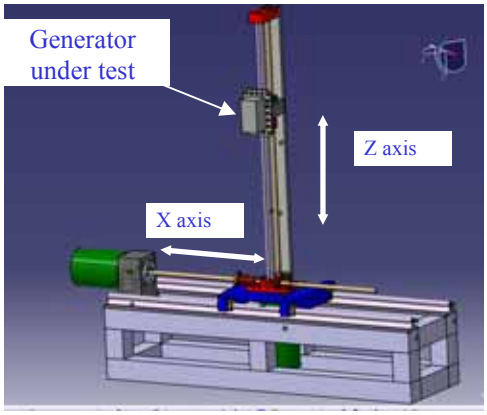

Fig 20 : Drawing of the walking simulator.

Figure 21 shows an electromotive force measurement at the generator coil terminals at 15 Hz. Results on useful electric power are not yet available because the present simulator is not appropriate to this « high » frequency range, since it was sized for low walking frequency (3 Hz maximum). But for the reason cited above (spring stiffness), the present generator prototype required higher frequencies. These results will be available soon.

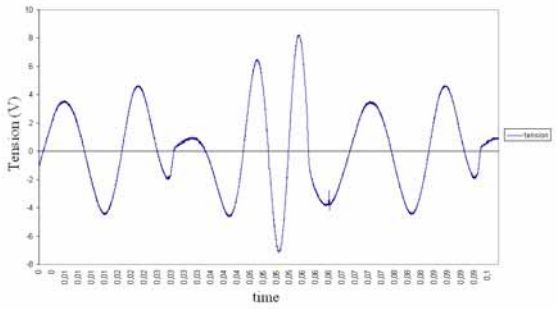

Figure 21 : EMF measurement at the generator coil terminals with an excitation frequency of 15 Hz.

VI. CONCLUSION

In this paper, we have presented an innovative electromechanical system for recovering energy from human movements with potential applications in recharging portable electronic devices accumulators. The proposed system is based on a linear tubular permanent magnet generator which provides a good robustness and extended lifetime.

Pre-design was performed using a multivariable and multiobjective optimization approach taking into account the mecanichal-electromagnetic-electrical coupling. We first detailed analytical modeling of four different linear permanent magnet and moving coil structures. Global optimization performed with a genetic algorithm showed the power production potential for a given total mass. Arelative proportionality exists between these two criteria.

It is also obvious that the hypothesis on the energy source will not be satisfied if the mechanical solicitation is too strong, i.e. beyond a total mass of a hundred of grams which corresponds to some 10 mW under typical walking conditions.

The recoverable power being proportional to the cube of the excitation frequency, powers far greater can be obtained when using other higher frequency vibrating sources.

Additional electrical loads should be studied, especially diode rectifiers feeded accumulators and PWM active control converters. This work is currently under study, optimization is made much more complex due to an aditional coupling at the electric level.

Unfortunately, there are few experimental results because of the difficulty in manufacturing adapted stiffness springs. However prototype's electromagnetic characteristics are in agreement with the optimization results and the recovered power should come as no surprise.

APPENDIX A : NOTATIONS

designation	**Symbole**
Magnet depth (mm)	W_M
Coil depth (mm)	W_C
α=magnet height / pole pitch	α
Coil height (mm)	h_C
Pole pitch (mm)	τ
Yoke 1 depth (mm)	Y_1
Yoke 2 depth (mm)	Y_2
Load resistance	r_L*
Total height (mm)	H
Average Power (W)	P_0
Mass (kg)	M
Spring stiffness (N/m)	k
Mobile Mass (kg)	m

APPENDIX B : VARIABLE BOUNDS

	Configurations 1-2		**Configuration 3**	
Designation	**Minimum**	**Maximum**	**Minimum**	**Maximum**
W_M	2	40	2	20
W_C	2	40	2	15
α	0	1	0	1
h_C	5	100	5	100
τ	5	50	6	20
Y_1	2	40	3	10
Y_2	2	40	2	20
r_L*	0	10	0	10
H	2	200	2	200

APPENDIX C : MAIN PROTOTYPE DIMENSIONS

designation	**symbol**	**Value**
Magnet tightness	W_M	8 mm
Magnet interior diameter	D_m	18 mm
Magnet exterior diameter	d_m	36 mm
Winding heigt	h	31 mm
Winding interior diameter	d_w	7 mm
Winding exterior diameter	D_w	18 mm
Spring stiffness	k	106 N/m
Spring diameter	d_s	10 mm
Spring free length	L_0	38.3 mm

VII. REFERENCES

[1] Starner T., "Human-Powered Wearable Computing", IBM Systems Journal, Vol. 35, pp. 618-629, 1996.

[2] Jansen A.J., Stevels A.L.N., "Human Power: A sustainable option for electronics", Electronics and the Environment, IEEE International Symposium Proceedings, 1999, pp. 215-218.

[3] Paradisco J., "Renewable Energy Sources for the Future of Mobile and Embedded Computing.", Computing Continuum Conference, San Francisco, CA, march 2000.

[4] Turri S., Miller D., Ben Ahmed H., Multon B., "Design of an electro-mechanical portable system using natural human body movements for electricity generation", EPE 2003, CDROM proc., Toulouse, sept. 2003.

[5] Wang J., Howe D., Geraint W., "Analysis and Design Optimization of an Improved Axially Magnetized Tubular Permanent-Magnet Machine", IEEE transactions on energy conversion, vol. 19, no. 2,june 2004.

[6] Deb K., Pratab A., Agrawal S. Heyarivau T. "A Fast and Elitist Genetic Algorithm: NSGA-II ". IEEE Transactions on evolutionary computation, volume 6, no. 2, pp 182-197, April 2002.

[7] J. Wang et al. : « A General Framework for the Analysis and Design of Tubular Linear Permanent Magnet Machines ». IEEE on Magnetics, vol. 35, NO. 3, May 1999. pp. : 1986-2000.

[8] N. Bianchi : « Analytical Field Computation of a Tubular Permanent-Magnet Linear Motor ». IEEE on Magnetics, vol. 36, NO. 5, May 2000. pp. : 3798-3801.

[9] N. Bianchi et al. : « Tubular Linear Permanent-Magnet Motors : An Overall Comparison ». IEEE on Industry Applications, vol. 39, NO. 2, March/April 2003. pp. : 466-475.